J. Fluid Mech. (1983), *vol.* 137, *pp.* 363–384
Printed in Great Britain

Nonlinear adjustment of a thin annular film of viscous fluid surrounding a thread of another within a circular cylindrical pipe

By P. S. HAMMOND†
Schlumberger-Doll Research, P.O. Box 307, Ridgefield, Connecticut 06877, U.S.A.

(Received 26 April 1983)

A nonlinear analysis, based on lubrication theory, is presented for the adjustment under surface tension of an initially uniform annular film of viscous fluid confined within a circular cylindrical pipe. The film surrounds a thread of another viscous fluid. Small axisymmetric interfacial disturbances of sufficiently long wavelength are found to grow, leading to the break-up of the initially continuous outer film into a number of isolated rings of fixed length on the pipe wall. The implications for the rupture of fluid threads surrounded by moderately thin films in confined geometries are discussed.

1. Introduction

When one fluid displaces another in a capillary tube, a thin film of the fluid initially present is often left behind on the tube walls (Taylor 1961). The details of this process depend on both the non-dimensional flow rate and the wetting properties of the two fluids and the pipe wall. Similar processes are thought to occur when oil and water displace one another in the pores and throats which constitute the flow channels in a porous rock.

The existence of such films has important consequences for later fluid transport and our modelling of it. Current microscopic models of two-phase flow in porous media, using the ideas of percolation theory, stress the importance of the connectivity of the fluid phases in determining the subsequent flow properties (for contrasting viewpoints see Larson, Scriven & Davis 1981; Koplik, Wilkinson & Willemsen 1983). Surface films can increase this connectivity, making available extra paths along which fluid rearrangements can take place.

Direct visualization of two-phase flows in realistic porous media is very difficult and the interpretation of measurements contentious. For example, there is little agreement on the wetting properties of rocks under reservoir conditions, or indeed on whether such quantities are well defined. Because of these observational difficulties, theoretical predictions based on well-understood physical processes are particularly valuable.

The main aim of this paper is to show that the time evolution of such systems can be successfully analysed using comparatively simple fluid mechanics. A second aim is a better understanding of the mechanisms of rearrangement and the equilibrium distributions of two phases within individual pores and throats of a porous medium. Most previous authors have analysed this problem using thermodynamic ideas

† Present address: Schlumberger Cambridge Research, P.O. Box 153, Cambridge CB2 3BE, England.

(Everett & Haynes 1972; Mohanty 1981). While such work is useful, it is essentially static and gives no information about time-dependent processes. Later we shall see that an understanding of these is important in deciding the accessibility of thermodynamically stable steady states.

While unconfined fluid threads have long been known to break up into spheres (e.g. Rayleigh 1892; Taylor 1934), little previous work has been done on the surface-tension instabilities of cylindrical films and threads when wall effects are important. Everett & Haynes (1972) have calculated the equilibrium shapes, and Goren (1962) and Hickox (1971) have performed linear stability analyses. Hickox's calculation was directed at an understanding of finite-Reynolds-number effects in coaxial flow and was restricted to the long-wavelength limit. He found that disturbances grow increasingly rapidly as their wavelength becomes shorter. Goren studied the stability of an annular film supported on a wire or on the inner wall of a pipe *in vacuo*. He considered arbitrary wavelengths and proved the existence of a fastest-growing disturbance with finite wavelength, showing that sufficiently short wavelengths decay because of the stabilizing effect of the longitudinal component of mean curvature.

In the nonlinear thin-film theory to be presented here the competition between the destabilizing effect of transverse curvature† at long wavelengths and the stabilizing effect of longitudinal curvature at short wavelengths again leads to the growth of disturbances with a finite axial lengthscale. The outer film eventually breaks up into a number of disconnected lobes. There is no simple relationship between the initial disturbance and the spacing and height of these final steady lobes. However, the axial extent of each lobe is fixed to be $2\pi \times$ (pipe radius), independent of the initial conditions, by the requirement that it be an equilibrium, constant-pressure shape (see §§4.1 and 4.3). It is also argued there that the spacing between adjacent lobes is no more than $2\pi \times$ (pipe radius). Using these observations, the maximum height of a lobe can be estimated from volume conservation.

2. Preliminary considerations

2.1. *Geometry and non-dimensional groups*

We consider an infinitely long cylindrical fluid thread of undisturbed radius b and viscosity $\lambda\mu$, surrounded by fluid of viscosity μ and situated concentrically in a circular pipe of radius a. Figure 1 shows the geometry in question. Gravitational effects are neglected, and it is assumed that no other body forces or pressure gradients are applied to the system so that the only driving force is due to surface tension γ acting at the interface $S(t)$ between the two fluids.

Although the systems that we want to model are very small‡ it is not immediately clear that inertia and buoyancy forces can be neglected. Taking $\lambda = O(1)$ and forming a Reynolds number for flow in the core thread using the pipe radius a as lengthscale and γ/μ as velocity, we obtain $\mathbb{R} = \rho a\gamma/\mu^2$, which is $O(10^3)$ for the parameter values given. The Bond number $\mathbb{B} = \Delta\rho g a^2/\gamma$, measuring the relative importance of gravity over surface tension, is then $O(10^{-2})$.

As we shall see in §3.1, the small driving pressure gradient and the high resistance to flow when the outer annular film is thin make all velocities much smaller than $O(\gamma/\mu)$. They are in fact $O((h/a)^3\gamma/\mu)$, where h is a typical film thickness. For

† Transverse curvature corresponds to the $(\,)R^{-1} - ((\,)R_\phi/R)_\phi R^{-1}$ terms in (2.12), longitudinal curvature to $-((\,)R_z)_z$.

‡ Typically for oil–water–sandstone systems $a = O(10^{-2})$ cm, $\mu = O(10^{-2})$ g cm^{-1} s^{-1}, $\lambda = O(1)$, $\gamma = O(20)$ dyn cm^{-1} and ρ, $\Delta\rho = O(1)$ g cm^{-3}.

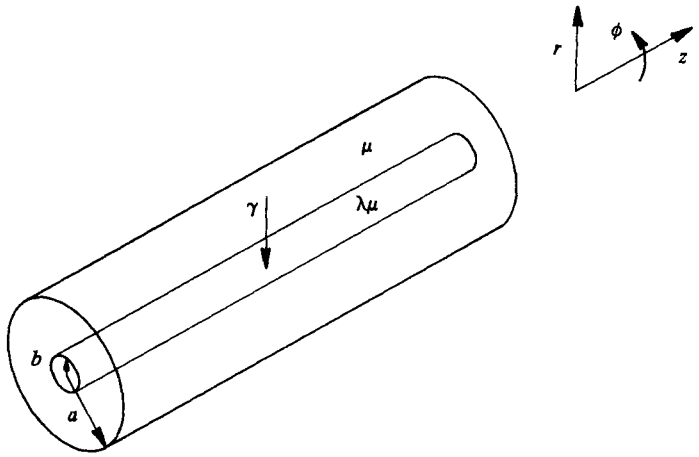

FIGURE 1. Defining sketch for basic thread geometry.

$h/a = O(10^{-2})$, $R = O(10^{-3})$, and inertia effects in the core are negligible. In the film, the effective Reynolds number is still smaller by virtue of the slowly varying geometry.

The Bond number estimated above is small, so we might expect that gravitational effects could be neglected. This idea must be examined carefully though. $B \ll 1$ certainly ensures that in a horizontal tube gravity does not appreciably change the cross-sectional shape of the core thread from a circle. At the same time though, the core, if less dense than the film, will tend to rise towards the upper wall of the pipe. Provided that rate of rise is small compared with the rate of surface-tension-driven adjustments, the neglect of gravity is justified. In §3.1 we shall argue that the pressure variations over a distance $O(a)$ due to surface tension acting at a distorted interface are $O((h/a)(\gamma/a))$. Over the same distance gravitational pressure variations are $O(\Delta\rho g a)$. The ratio of these two is $O((h/a)^{-1}\Delta\rho g a^2/\gamma)$, and provided that this quantity is small then buoyancy-driven flows are weak compared with those driven by surface tension. We require $B \ll O(h/a)$, which for the quoted parameter values leads to the restriction $h/a \gg O(10^{-2})$. This is only just compatible with the requirement that the outer film be thin, but for smaller pipe radii, e.g. $a = O(10^{-3}\text{ cm})$, which is not untypical of the radii of the smaller pores in a sandstone, $B = O(10^{-4})$. Gravity may then be neglected if $h/a \gg O(10^{-4})$; in practice, hardly a severe constraint.

2.2. *Governing equations*

We write the fluid pressure and velocity as p, $\boldsymbol{u}$ in the outer fluid film and P, U in the core, and use cylindrical coordinates (r, z, ϕ) with associated velocity components (u, w, v) in the film and (U, W, V) in the core. The interface $S(t)$ is given by

$$r = R(z, \phi, t) = a - h(z, \phi, t), \tag{2.1}$$

and the governing equations and boundary conditions to be satisfied in any time evolution of the system as as follows:

$$\nabla \cdot \boldsymbol{U} = 0, \tag{2.2}$$

$$\lambda\mu\nabla^2\boldsymbol{U} = \nabla P \tag{2.3}$$

in the core, $R > r \geqslant 0$, and

$$\nabla \cdot \boldsymbol{u} = 0, \tag{2.4}$$

$$\mu\nabla^2\boldsymbol{u} = \nabla p \tag{2.5}$$

in the film, $a > r > R$. We require no slip at the pipe wall,

$$\boldsymbol{u} = 0 \quad \text{at} \quad r = a, \tag{2.6}$$

continuity of velocity at the interface,

$$\boldsymbol{u} = \boldsymbol{U} \quad \text{at} \quad r = R, \tag{2.7}$$

and continuity of tangential stress there with the normal component jumping by an amount given by Laplace's formula,

$$\boldsymbol{\sigma}\cdot\boldsymbol{n} - \boldsymbol{\Sigma}\cdot\boldsymbol{n} = \gamma\kappa\boldsymbol{n} \quad \text{at} \quad r = R. \tag{2.8}$$

The stress tensors are given by

$$\boldsymbol{\sigma} = -p\boldsymbol{I} + \mu(\nabla\boldsymbol{u} + \nabla\boldsymbol{u}^{\mathrm{T}}) \tag{2.9}$$

and

$$\boldsymbol{\Sigma} = -P\boldsymbol{I} + \lambda\mu(\nabla\boldsymbol{U} + \nabla\boldsymbol{U}^{\mathrm{T}}), \tag{2.10}$$

and the outward normal to the core is

$$\boldsymbol{n} = \left(\hat{\boldsymbol{r}} - R_z\hat{\boldsymbol{z}} - \frac{R_\phi}{R}\hat{\boldsymbol{\phi}}\right), \tag{2.11}$$

where subscripts denote differentiation and $\hat{\boldsymbol{r}}$, $\hat{\boldsymbol{z}}$ and $\hat{\boldsymbol{\phi}}$ are unit vectors in the r-, z- and ϕ-directions. The mean curvature κ is then

$$\kappa = \nabla\cdot\hat{\boldsymbol{n}} = (\,)R^{-1} - ((\,)R_z)_z - \left((\,)\frac{R_\phi}{R}\right)_\phi R^{-1}, \tag{2.12}$$

where $\hat{\boldsymbol{n}} = \boldsymbol{n}/|\boldsymbol{n}|$ and

$$(\,) = \left(1 + R_z^2 + \left(\frac{R_\phi}{R}\right)^2\right)^{-\frac{1}{2}}. \tag{2.13}$$

The Stokes equations (2.2)–(2.5) and boundary conditions (2.6)–(2.8) are instantaneous in that the velocity and stress fields at some time t depend only on the current position of the interface. A simple equation for the evolution of an interface described by (2.1) can be found in terms of the instantaneous flow field as follows. The kinematic requirement of no flux of fluid through the interface may be written

$$u = -\frac{\mathrm{D}h}{\mathrm{D}t} = -h_t - \boldsymbol{u}\cdot\nabla h \quad \text{at } S(t), \tag{2.14}$$

which may be recast as

$$h_t = -u - wh_z - v\frac{h_\phi}{a-h} = -\boldsymbol{u}\cdot\boldsymbol{n} \quad \text{at } S(t). \tag{2.15}$$

By (2.7), $\boldsymbol{u}$ could be replaced by $\boldsymbol{U}$ in the above, but it is most convenient in the sequel to work with the film velocity. Mass conservation for the annular wedge of outer (film) fluid between z and $z+\mathrm{d}z$ and ϕ and $\phi+\mathrm{d}\phi$ requires

$$\int_{\text{surface of wedge}} \boldsymbol{u}\cdot\mathrm{d}\boldsymbol{S} = 0, \tag{2.16}$$

which relates $\boldsymbol{u}\cdot\boldsymbol{n}$ at $S(t)$ to the volume flux in the film. Equation (2.15) can then be written as

$$h_t = -\frac{1}{a-h}\left(\frac{\partial Q_w}{\partial z} + \frac{1}{a}\frac{\partial Q_v}{\partial\phi}\right), \tag{2.17}$$

where

$$Q_w(z,\phi,t) = \int_{a-h(z,\phi,t)}^{a} w(r,z,\phi,t)\,r\,\mathrm{d}r \tag{2.18}$$

and

$$Q_v(z,\phi,t) = \int_{a-h(z,\phi,t)}^{a} v(r,z,\phi,t)\,a\,\mathrm{d}r. \tag{2.19}$$

Hence the time evolution of the interface is completely determined if we can find the film axial and azimuthal velocities w, v. This problem is addressed in §3, but first we summarize the results of a linearized stability analysis of (2.2)–(2.8), reported in more detail in Hammond (1982).

2.3. *Linear stability analysis*

The time evolution of small interface disturbances of the form

$$R = b(1+\beta e^{\alpha t+ikz}), \tag{2.20}$$

with $|\beta| \ll 1$ and $0 \leqslant k < \infty$, is most easily found using the kinematic boundary condition (2.14) directly rather than in the integral form (2.17). Linearization about a basic state of rest and use of the general solution for Stokes flow in cylindrical geometry given by Happel & Brenner (1965, p. 77) eventually yields an unwieldy expression for $F = (b\mu/\gamma)\alpha$ as a function of $kb, a/b$ and λ. From this can be retrieved, as limiting cases, the results of Rayleigh (1892) for a thread *in vacuo* and of Tomotika (1935) for an inviscid thread in unbounded viscous fluid. In both cases the fastest-growing mode has infinite wavelength.

To interpret the behaviour of $F(kb, a/b, \lambda)$ further we examine the interface curvature, which, through surface tension, supplies the only driving force for the flow. Let us for a moment consider non-axisymmetric perturbations, including a term $e^{im\phi}$, $m = 0, 1, 2, \ldots$, in (2.20). Substitution of this augmented form of (2.20) in (2.12) and linearization gives

$$\kappa = \frac{1}{b}(1+\beta((kb)^2+m^2-1)\, e^{\alpha t+i(kz+m\phi)}). \tag{2.21}$$

Writing $N = (kb)^2+m^2-1$, it is easy to see that the normal stress jump across the interface required by (2.8) sets up a flow which reduces the size of the disturbance if $N > 0$ and increases it if $N < 0$. For $m > 1$, N is always positive, while for $m = 1$ it is zero when $kb = 0$ and positive elsewhere. Within this linearized analysis then, non-axisymmetric perturbations are stable and hence uninteresting (the neutrally stable case $kb = 0$, $m = 1$ corresponds to uniform displacement of the thread from the tube centreline without change of shape). Although there is no guarantee that this conclusion will be true for finite-amplitude disturbances, for simplicity from here on we will neglect all non-axisymmetric effects, setting v, V and $\partial/\partial\phi = 0$. There is no difficulty in principle in extending the nonlinear theory below to include non-axisymmetric disturbances, but the computational effort increases enormously.

As $|kb| \to \infty$, $N \to \infty$, indicating that short waves are stable. Such disturbances appear locally as wrinkling on an almost flat surface which can only increase its area. On thermodynamic grounds such disturbances decay. It is possible, however, for sufficiently long waves to decrease the thread's area, as was shown by Rayleigh (1892) and Tomotika (1935). There is no analogous instability of unbounded plane interfaces, because their area can only be increased by small perturbations. The destabilizing influence of the $(\,)R^{-1}$ term in (2.12) is absent.

Numerical evaluation of $F(kb, a/b, \lambda)$ confirms both the above observations and the conclusions of Goren (1962) and Tomotika (1935) that the effect of boundaries or of finite viscosity ratio is to make the wavelength of the fastest-growing mode finite.

An interesting and original set of limits can be found by taking $(a-b)/b \ll 1$ so that the outer film is thin. Setting

$$a = b(1+\eta) \quad \text{with} \quad 0 < |\beta| \ll \eta \ll 1 \tag{2.22}$$

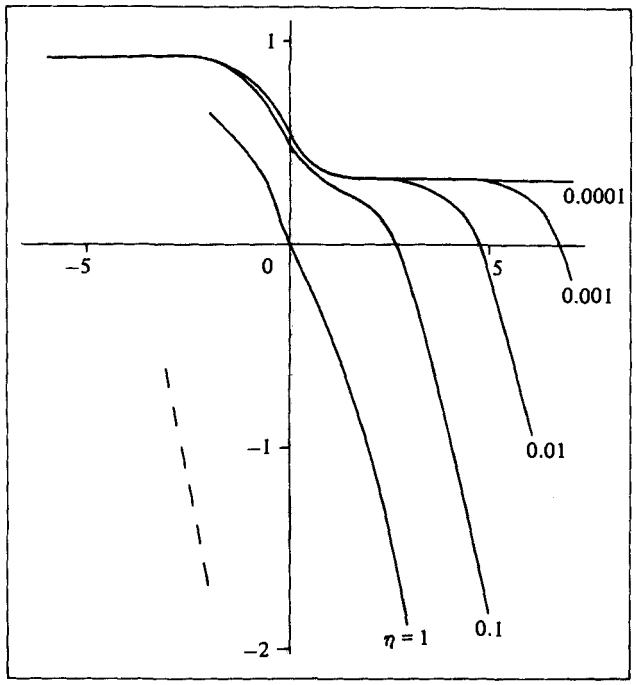

FIGURE 2. Log_{10} ($100\eta^{-3} \times$ maximum growth rate from linear theory) plotted against $\log_{10}(\eta\lambda)$ for various values of η. Notice the two flat regions which appear on each graph when $\eta < 0.1$, showing that the growth rate is then independent of the viscosity ratio λ. These regions correspond to, and are in good numerical agreement with, the thin-film limits (2.23) and (2.24). The dashed line has slope -1. All the graphs become parallel to it as $\eta\lambda \to \infty$, showing that then it is the core flow alone which controls the growth rate of small disturbances.

and expanding F, we obtain to leading order

$$F \sim \frac{\eta^3}{3}(kb)^2(1-(kb)^2) \quad \text{when} \quad \lambda \ll \eta^{-1}, \tag{2.23}$$

$$F \sim \frac{\eta^3}{12}(kb)^2(1-(kb)^2) \quad \text{when} \quad \eta^{-1} \ll \lambda \ll \eta^{-3} \tag{2.24}$$

and

$$F \sim \frac{(kb)^2-1}{2\lambda\left(1+(kb)^2\left(1-\dfrac{I_0^2(kb)}{I_1^2(kb)}\right)\right)} \quad \text{when} \quad \eta^{-3} \ll \lambda. \tag{2.25}$$

Equation (2.25) is identical with the (non-dimensional) growth rate found by Rayleigh for a thread *in vacuo*, indicating that for sufficiently large core viscosities the hydrodynamics of the thin outer film are not important in determining the rate of growth of interface disturbances. Equations (2.23) and (2.24) exhibit a strong dependence on the (non-dimensional) film thickness, which suggests that the dynamics of the outer fluid become important as η or λ decrease. Indeed (2.23) can be obtained in the thin-film limit (2.22) from Goren's growth-rate relation for a wall-supported annular thread *in vacuo*, indicating that the dynamics of the core fluid play no part in determining the growth rate of interfacial disturbances when the outer film is sufficiently thin or the core sufficiently mobile. We shall examine the film-region

dynamics in §3, and an explanation for the appearance of the η^3 factor in (2.23) will be given.

In both (2.23) and (2.24) the fastest-growing modes have finite wavelength $2\frac{1}{2}\pi b$, which is comparable to the pipe diameter; in (2.25) the fastest-growing wavelength is infinite. Figure 2 shows the logarithm of the growth rate of the fastest-growing mode plotted against $\log_{10}\eta\lambda$ for various non-dimensional film thicknesses η. The three regimes described above are clearly visible.

3. Nonlinear thin-film analysis

Linear stability analysis has shown that, for thin outer fluid films and all except the largest values of λ, the fastest-growing interface perturbations have wavelength comparable to the pipe radius a. This suggests that when investigating their growth to an amplitude comparable to the undisturbed film thickness we should write the film thickness $h(z,t)$ as in (2.1) with $h/a \ll 1$, allow changes in h to be as large as its undisturbed value, and take $a\,\partial/\partial z = O(1)$. The film radial lengthscale is then much smaller than the axial lengthscale, and this makes a number of simplifying approximations possible. In the core axial and radial lengthscales are comparable and $O(a)$, and so the dynamical equations cannot be approximated there.

3.1. *Orders of magnitude*

First consider the core fluid to be an inviscid incompressible fluid, i.e. $\lambda = 0$. Under the assumption of slow flow, the core pressure P is constant, and by suitable choice of reference pressure we may set $P = 0$. Surface tension acting at the interface causes there to be a jump in normal stress across it proportional to the local mean curvature κ. Because the core is inviscid it cannot support any non-uniform stresses, and using $P = 0$ we see that $\boldsymbol{\Sigma} = 0$ everywhere. Then from (2.8)

$$\sigma_{nn} = \gamma\kappa \quad \text{on } S(t). \tag{3.1}$$

Continuity of tangential stress requires

$$\sigma_{nt} = 0 \quad \text{on } S(t). \tag{3.2}$$

With $S(t)$ given by (2.1), expanding (2.12) for $|h/a|$, $|h_z|$ and $|ah_{zz}| \ll 1$, we obtain

$$\kappa = \frac{1}{a} - \frac{1}{a}\left(\frac{h}{a} + ah_{zz}\right) + O\left(\frac{h^2}{a^3}, \frac{h_z^2}{a}, h_{zz}h_z^2\right). \tag{3.3}$$

In addition to this geometrical approximation, the small rate of change of film thickness with z and the thinness of the film allow us to use plane two-dimensional lubrication theory to describe the flow there. The pressure is constant across the film and in the normal stress boundary condition the dominant balance is between pressure and surface tension, the viscous normal stresses being smaller by $O(h/a)^3$. From (3.1) the pressure variation along the film is

$$p(r,z,t) = p(z,t) = -\gamma\kappa(z,t). \tag{3.4}$$

Using (3.3), we see that in the film there is a uniform pressure $-\gamma/a$ about which variations in the core radius cause small $O((h/a)\gamma/a)$ pressure perturbations. The associated flows cause adjustments of the interface on a timescale given by

$$T_{\text{film}} = O\left(\frac{h}{u}\right) = O\left(\left(\frac{h}{a}\right)^{-3}\frac{a\mu}{\gamma}\right), \tag{3.5}$$

using the standard estimates obtained from the film axial-momentum and mass-conservation equations

$$w = O\left(\frac{h^2 p_z}{\mu}\right), \quad u = O\left(\frac{h}{a} w\right), \tag{3.6}$$

and, from (3.3) and (3.4),

$$p_z = O\left(\left(\frac{h}{a}\right)\frac{\gamma}{a^2}\right). \tag{3.7}$$

This very long adjustment time is a consequence of the small driving pressure gradient and the large resistance to viscous flow in narrow channels.

Now consider the core fluid to have finite viscosity. For λ not too large the basic flow in the film should be much as described above, driven by a small but significant pressure gradient there. Via the interfacial velocity and stress continuity conditions it will set up a flow in the core, which couples back to the film, changing the basic velocity and pressure fields there. These disturbances are small provided that

$$\lambda\left(\frac{h}{a}\right) \ll 1, \tag{3.8}$$

as we shall now show.

In the case $\lambda = 0$, the lubrication theory solution for the film axial velocity is non-zero at the interface, while the tangential stress vanishes there. Assuming that when λ is finite w is still non-zero at the interface, continuity of axial velocity requires a core flow with velocities

$$|\boldsymbol{U}| = O(w) = O\left(\left(\frac{h}{a}\right)^3 \frac{\gamma}{\mu}\right) \tag{3.9}$$

and associated stresses of order

$$|\boldsymbol{\Sigma}| = O\left(\frac{\lambda\mu|\boldsymbol{U}|}{a}\right) = O\left(\lambda\left(\frac{h}{a}\right)^3 \frac{\gamma}{a}\right). \tag{3.10}$$

Because the radial component of the film velocity is at most $O((h/a)w)$ the radial component of $\boldsymbol{U}$ must vanish (at leading order) at the interface, but both the tangential and normal stress components in the core will in general be non-zero there and will be given in order of magnitude by (3.10). Hence, provided that $\lambda(h/a)^2 \ll 1$, pressure variations in the core are small compared with those in the film. The non-zero core tangential stress at $S(t)$ drives a flow in the film with axial velocity $O(\lambda(h/a)w)$. And from the normal-stress jump condition we see that core pressure variations require a pressure perturbation in the film of $O(\lambda(h/a)^3\gamma/a)$, which sets up an axial velocity of $O(\lambda(h/a)^2 w)$. Both these flows are small compared with w if $\lambda(h/a) \ll 1$, giving (3.8).

3.2. *Formal analysis when* $\lambda(h/a) \ll 1$

The arguments given above can be made more formal by expressing them in the language of perturbation theory. Introducing the non-dimensional undisturbed film thickness

$$\epsilon = \frac{a-b}{a}, \tag{3.11}$$

we examine (2.1)–(2.14) in the limit $\epsilon \ll 1$, $\epsilon\lambda \ll 1$, $h(z,t)/\epsilon a$ and $a\partial/\partial z = O(1)$. Prompted by the estimates of §3.1, we introduce the following variables, denoting non-dimensional quantities with an asterisk. In the film we take independent variables

$$z^* = \frac{z}{a}, \quad y^* = \frac{a-r}{\epsilon a}, \quad t^* = \frac{t}{\epsilon^{-3}(a\mu/\gamma)}, \tag{3.12}$$

so that from (2.1) the interface may be described by

$$y^* = \frac{h(z,t)}{\epsilon a} = H^*(z^*, t^*), \tag{3.13}$$

with $H^* = O(1)$. The instantaneous velocity and pressure fields are written as

$$w = \epsilon^3 \frac{\gamma}{\mu} w^*(y^*, z^*), \quad u = \epsilon^4 \frac{\gamma}{\mu} u^*(y^*, z^*), \quad p = \frac{\gamma}{a}(-1 + \epsilon p^*(y^*, z^*)), \tag{3.14}$$

and the film volume flux as

$$Q_w = \epsilon^4 \frac{a^2 \gamma}{\mu} Q^*(z^*). \tag{3.15}$$

In the core we write

$$\boldsymbol{x} = a\boldsymbol{x}^*, \tag{3.16}$$

$$\boldsymbol{U} = \epsilon^3 \frac{\gamma}{\mu} \boldsymbol{U}^*(\boldsymbol{x}^*) \tag{3.17}$$

and

$$P = \epsilon^3 \lambda \frac{\gamma}{a} P^*(\boldsymbol{x}^*), \quad \boldsymbol{\Sigma} = \epsilon^3 \lambda \frac{\gamma}{a} \boldsymbol{\Sigma}^*(\boldsymbol{x}^*). \tag{3.18}$$

Substituting (3.12)–(3.15) in (2.4) and (2.5), we obtain

$$w_z - u_y = -\epsilon u + O(\epsilon^2), \tag{3.19}$$

$$p_z - w_{yy} = -\epsilon w_y + O(\epsilon^2), \tag{3.20}$$

$$p_y = -\epsilon^2 u_{yy} + O(\epsilon^3), \tag{3.21}$$

dropping asterisks because all quantities are now non-dimensional. The leading corrections in (3.19) and (3.20) come from the expansion of $1/r$ factors in ∇ as $1 + \epsilon y + O(\epsilon^2)$. In physical terms, the film geometry appears two-dimensional rather than axisymmetric. In the core we obtain

$$\nabla \cdot \boldsymbol{U} = 0, \quad \nabla^2 \boldsymbol{U} = \nabla P. \tag{3.22}$$

No slip at the pipe wall requires

$$w(0,z) = u(0,z) = 0, \tag{3.23}$$

and continuity of both velocity components at $S(t)$ requires

$$W(1 - \epsilon H(z,t), z) - w(H(z,t), z) = 0, \quad U(1 - \epsilon H(z,t), z) = \epsilon u(H(z,t), z). \tag{3.24}$$

Assuming that $\boldsymbol{U}$ is sufficiently regular that it can be expanded about $r = 1$, we may transfer the core velocity boundary values there to obtain

$$W(1,z) - w(H(z,t), z) = O(\epsilon), \quad U(1,z) = O(\epsilon). \tag{3.25}$$

To form the stress boundary conditions we need the normal and tangent vectors on $S(t)$:

$$\boldsymbol{n} = \hat{\boldsymbol{r}} + \epsilon H_z \hat{\boldsymbol{z}}, \quad \boldsymbol{t} = -\epsilon H_z \hat{\boldsymbol{r}} + \hat{\boldsymbol{z}}. \tag{3.26}$$

Continuity of tangential stress requires

$$\epsilon^2((1 - \epsilon^2 H_z^2)(-w_y + \epsilon^2 u_z) + 2\epsilon^2 H_z(w_z + u_y)) = \epsilon^3 \lambda((1 - \epsilon^2 H_z^2)(U_z + W_r) + 2\epsilon H_z(W_z - U_r)) \quad \text{at } S(t), \tag{3.27}$$

from which we obtain, again transferring boundary conditions,

$$w_y(H,z) = -\epsilon\lambda(U_z + W_r)_{(1,z)} + O(\epsilon^2, \epsilon^2\lambda). \tag{3.28}$$

The normal-stress boundary condition becomes

$$\begin{aligned}\epsilon^3\lambda(-|\boldsymbol{n}|^2 P + 2(U_r + \epsilon H_z(U_z + W_r) + \epsilon^2 H_z^2 W_z)) \\ -|\boldsymbol{n}|^2 + \epsilon|\boldsymbol{n}|^2 p - (-2\epsilon^3 u_y + 2\epsilon^5 H_z(u_z - w_y) + 2\epsilon^5 H_z^2 w_z) \\ = -|\boldsymbol{n}|^2((1+\epsilon^2 H_z^2)^{-\frac{1}{2}}(1-\epsilon H)^{-1} + \epsilon(1+\epsilon^2 H_z^2)^{-\frac{3}{2}} H_{zz}) \quad \text{at } S(t),\end{aligned} \tag{3.29}$$

from which we obtain

$$p(H(z,t),z) = -(H + H_{zz}) + O(\epsilon^2, \epsilon^2\lambda). \tag{3.30}$$

The set of equations and boundary conditions above suggest that we pose asymptotic expansions for the dependent variables of the form

$$\psi \sim \psi_0 + \epsilon\psi_{10} + \epsilon\lambda\psi_{01}, \tag{3.31}$$

although only the zeroth-order terms will be considered here. From (3.19)–(3.22) we then obtain

$$w_{0z} - u_{0y} = 0, \tag{3.32}$$

$$p_{0z} - w_{0yy} = 0, \tag{3.33}$$

$$p_{0y} = 0, \tag{3.34}$$

$$\boldsymbol{\nabla}\cdot\boldsymbol{U}_0 = 0, \quad \boldsymbol{\nabla}P_0 = \boldsymbol{\nabla}^2\boldsymbol{U}_0, \tag{3.35}$$

subject, using (3.23), (3.25), (3.28) and (3.30), to

$$w_0(0,z) = u_0(0,z) = 0, \tag{3.36}$$

$$W_0(1,z) = w_0(H(z,t),z), \quad U_0(1,z) = 0, \tag{3.37}$$

$$w_{0y}(H(z,t),z) = 0 \tag{3.38}$$

and

$$p_0(H(z,t),z) = -H - H_{zz}. \tag{3.39}$$

The flow in the film is then given to leading order by

$$p_0 = p_0(z) = -H - H_{zz}, \tag{3.40}$$

$$w_0 = \tfrac{1}{2}p_{0z}(y^2 - 2Hy), \tag{3.41}$$

$$u_0 = \frac{1}{2}\left(p_{0zz}\left(\frac{y^3}{3} - Hy^2\right) + p_{0z}H_z y^2\right), \tag{3.42}$$

and expansion and approximation in (2.18) yields

$$Q_0 = -\tfrac{1}{3}H^3 p_{0z}. \tag{3.43}$$

Finally from (2.17), (3.39) and (3.43) we obtain the following evolution equation for interface disturbances:

$$H_t = -\tfrac{1}{3}(H^3(H_{zzz} + H_z))_z. \tag{3.44}$$

There is no need to solve for the core flow, although it can be found if desired, for example by making a Fourier decomposition of $w_0(H(z,t),z)$ and using the general solution of Happel & Brenner (1965, p. 77). The derivation of (3.44) is independent of the detailed mechanics of the core region, proving the assertion of §2.3 that for ϵ and $\epsilon\lambda$ sufficiently small the dynamics of the film region control the evolution of

interface disturbances while the core responds passively. This is reflected in (2.23) and the leftmost part of the growth-rate curves of figure 2, where we see that the growth rate of small disturbances is independent of λ and so of the core dynamics.

4. Solution of interface evolution equation

4.1. *Analytical investigations*

There is little that can be done analytically with (3.44). Putting $H = 1+\beta e^{\alpha t+ikz}$ with $|\beta| \ll 1$ and linearizing yields

$$\alpha = \tfrac{1}{3}k^2(1-k^2), \tag{4.1}$$

from which (2.23) can be recovered when dimensional and scaling factors are replaced.

Steady states satisfy

$$H^3(H_{zzz}+H_z) = 3Q_0, \tag{4.2}$$

where Q_0 is the film volume flux introduced at (3.43) and is constant. Acceptable solutions must have $H \geqslant 0$ everywhere. If $Q_0 \neq 0$ then $H > 0$, for otherwise a volume source or sink would be required at the zero of H. Suppose now that H is bounded above also so that $M > H(z) > m > 0$. We can without loss of generality take $Q_0 > 0$. Then

$$\frac{3Q_0}{m^3} > \frac{\mathrm{d}}{\mathrm{d}z}(H_{zz}+H) > \frac{3Q_0}{M^3} > 0,$$

which we may integrate to give

$$\frac{3Q_0}{m^3}z+C_1 > H_{zz}+H > \frac{3Q_0}{M^3}z+C_2,$$

where C_1 and C_2 are constants. For large $|z|$ the upper and lower bounds on H_{zz} grow linearly, and integrating twice more we find that H is bounded above and below by functions that grow like z^3. This is incompatible with the assumption that H is finite for all z. We do not consider these unbounded solutions with $Q_0 \neq 0$ further because they do not seem suitable to describe an infinite thread in a stationary pipe with no applied body forces.

Away from any zeros of H, steady states with $Q_0 = 0$ take the form

$$H = A+B\cos(z+\delta), \tag{4.3}$$

with A, B and δ constant. For $A > |B| > 0$ this is the neutrally stable mode of linear stability theory, which can also be interpreted as the small-amplitude limit of the family of unduloids which are the axially symmetric constant-pressure surfaces of finite amplitude. Everett & Haynes (1972) in their discussion of capillary condensation have shown by thermodynamic arguments that such menisci are stable.

The possibility of H having a zero remains, and a power-series solution shows that near such a singular point of (4.2) $H \sim \nu(z-z_0)^\rho$, with ν constant and $\rho = 0$, 1 or 2. This is compatible with (4.3) provided that $|B| \geqslant |A|$; $\rho = 2$ corresponds to $|B| = A > 0$, $\rho = 1$ to $|B| > |A|$, and $\rho = 0$ to $A = B = 0$.

Suppose now we look for steady solutions of (3.44) that are not 2π-periodic because, for example, some incommensurate external lengthscale has been imposed. As it stands (4.3) is not then a possible solution, but there seems to be no reason why H should not be piecewise of the form (4.3) with $|B| \geqslant |A|$, these sections being separated by regions where $H \equiv 0$. In §4.2 we shall see that numerical solutions of (3.44) approach such a form at large times, and in §4.3 we shall give an asymptotic solution of (3.44) which indicates that an infinite time is required for H to become zero

anywhere. Although the piecewise-zero solutions discussed above are not attained in any finite time, a solution of (3.44) can approach them arbitrarily closely as $t \to \infty$.

4.2. *Numerical investigations*

Before integrating (3.44) numerically we must supplement it with some boundary conditions, the most convenient choice being to take H periodic with period L. Because of the fixed and finite axial lengthscale of the steady solution (4.3), we expect that provided $L \gg 2\pi$ the evolution towards such shapes will not be too strongly dependent on L. This assumption must be checked by examining various values of L, which is, of course, an artificially imposed lengthscale.

Computations were in fact performed with the more restrictive but also more economical set of boundary conditions

$$\frac{\partial^{2j+1} H}{\partial z^{2j+1}} = 0 \quad (j = 0, 1, 2, \ldots; \; z = 0, \tfrac{1}{2}L), \tag{4.4}$$

corresponding to H even with period L and reflectionally symmetric about $z = \frac{1}{2}L$. It is easily seen from (3.44) that a disturbance initially satisfying (4.4) does so at all later times.

Equation (3.44) was solved numerically by replacing the spatial derivatives with finite differences, generating a system of coupled ordinary differential equations for the time evolution of H at set of mesh points. This procedure is sometimes known as the method of lines. The resulting ODE set is stiff and it is necessary to employ an implicit time-stepping method to solve it. Gear's method, as implemented in the Numerical Algorithms Group (NAG) subroutine library, was chosen and proved to very effective. A discussion of the numerical difficulties of stiff systems and methods for treating them is given in Hall & Watt (1976, chap. 11).

Equation (3.44) was integrated numerically for a variety of initial conditions and various values of L. Computer-time restrictions at Cambridge limited the size of system that could be solved to a maximum of 96 spatial points, and the limited spatial resolution then forced $L \leqslant 6\pi$. 24- and 48-point programs were also run and gave similar results. Subsequently at SDR, on the suggestion of a referee, some computations with 400 spacial points were made, allowing values of L as large as 40π to be investigated. For small and moderate times ($t < O(300)$) the same general behaviour was seen for small and large L. However, in their very-long-time behaviour the solutions for $L > O(10\pi)$ appeared to be less strongly constrained than those for smaller values of L. We discuss this observation further in §4.3.

For all initial conditions and all values of L the following behaviour was seen. Disturbances stable according to linear theory decayed, even for finite initial amplitude. With $L > 2\pi$, linearly unstable disturbances grew and reached a quasi-steady state consisting of a number of lobes of the form (4.3) separated by short adjustment regions where H was small. The same general form was seen for all initial conditions. It was not possible to follow this quasi-steady state to a final equilibrium because of the very slow adjustments taking place and the numerical difficulty of resolving the short axial lengthscales (in particular the large values of H_{zzz}) which developed in the adjustment regions where the interface was approaching the wall. In §4.3 an approximate analytical treatment of this final stage of adjustment will be given.

Most runs were made with initial conditions of the form

$$H(z, 0) = 1 + \beta \cos \frac{2\pi z}{L}, \tag{4.5}$$

although starting from $H = 1 +$(small random noise) gave qualitatively similar results at large times. For unstable disturbances $L > 2\pi$, as the perturbation grows flattening of the interface takes place where it is approaching the wall. Because the resistance to flow increases very rapidly ($\sim H^3$) as H decreases and the driving pressure gradient is small where the interface is almost flat, significant fluid motion occurs only near the ends of the flattening region where the interface is curving away from the wall. Fluid in the rest of the flattened region is almost stationary. The expulsion of fluid from its ends causes the flattened region to lengthen, as can be seen in figure 3(*a*). In the region where expelled fluid collects, H is large, so resistance to flow is small and adjustments can occur rapidly compared with the timescale for expulsion of fluid from the flattening zone. Any departures of the interface shape from a constant-pressure form given by (4.3) relax quickly. The region between this lobe and the flattened part of the film continues to thin, effectively isolating the two zones. Adjustments in the flattened zone then take place, duplicating those described above, leading to the break-up of the film into a sequence of constant-pressure lobes separated by short regions where the z-derivative of interface curvature is large and a significant pressure adjustment takes place. Figure 3(*b*) shows this secondary-lobe formation.

Apart from the formation of a moderately large lobe at $z = 0$ there is little relation between lobe size and initial conditions. In particular, there is no tendency for all the film fluid in $[0, L]$ to be gathered up into a single lobe. A succession of large and small lobes are formed. The large ones approach the wall almost tangentially ($|B| = -A$ in (4.3)) while the small lobes have finite gradient there and seem to be draining into their larger neighbours. Figures 4(*a*, *b*) illustrate these quasi-steady states. This drainage process can be understood from (3.39) and (4.3). Large lobes with axial length $> \pi$, and so $A > 0$ in (4.3), have negative pressure, while those with length $< \pi$, and so $A < 0$, are at a positive pressure. There will thus be a flux of fluid from small to large, and if the gap joining them does not thin too rapidly this will lead to the complete drainage of the small lobe. Alternatively, if the gap region thins sufficiently quickly, the small lobe does not drain completely and both large and small lobes persist for all time. We now examine (3.44) in the gap region and construct a solution valid at large times which predicts complete drainage of the small lobe.

4.3. *Long-time behaviour of a draining lobe*

This section is based on Jones & Wilson's (1978) analysis of the draining film beneath a droplet settling towards a fluid interface. Wu & Weinbaum (1982) have made use of similar ideas to discuss the long-time drainage of the fluid lobe trapped against a wall by a flexible cell. Here, once the film has developed into a number of almost independent lobes, the timescales for adjustment of different parts of the interface become widely separated. Certain regions can then be treated as quasi-steady, and the PDE (3.44) replaced by an ODE with known solutions.

We work with the scaled equation (3.44) so that the basic film thickness is $O(1)$. Consider now the narrow gap region seen in the numerical solutions joining two lobes, and let its height be $O(\bar{\epsilon}) \ll 1$ (i.e. $H = O(\bar{\epsilon})$). The change in curvature across this region is observed from the numerical work to be $O(1)$, and so its axial lengthscale must be $O(\bar{\epsilon}^{\frac{1}{2}})$.

From (3.44) we estimate the timescale for relaxation of an $O(1)$ perturbation to H in the large filling lobes to be $O(1)$, so for large times H will there have the constant-pressure form (4.3). Anticipating a later conclusion, the draining lobe has height $O(\bar{\epsilon}^{\frac{1}{2}})$ and length $O(1)$. Its relaxation time is then $O(\bar{\epsilon}^{-\frac{3}{2}})$. In the gap linking

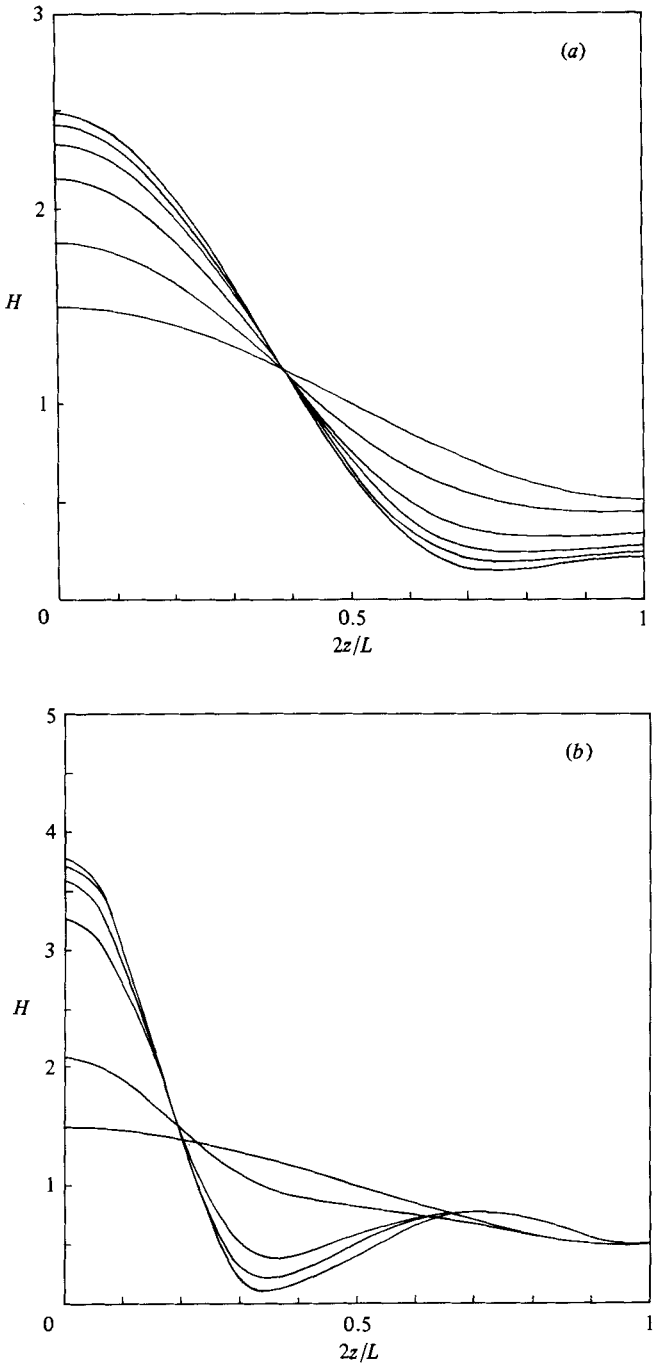

FIGURE 3 (*a*, *b*). Initial stages of adjustment for (*a*) $L = 2\frac{1}{2}\pi$, the fastest-growing mode of linear theory, $t = 0, 6, 18, 30, 42, 54$; and (*b*) $L = 6\pi$, $t = 0, 6, 18, 30. 60$. The initial disturbances are given by (4.5) with $\beta = 0.5$.

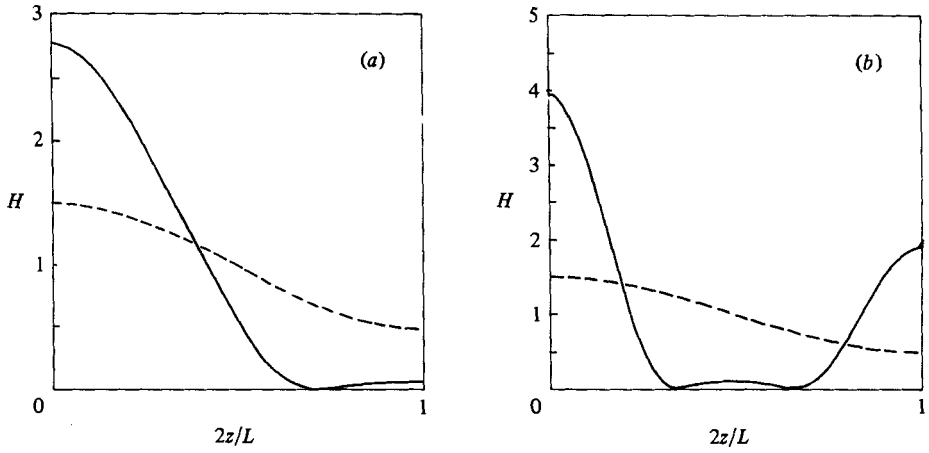

FIGURE 4(*a*, *b*). Quasi-steady long-time behaviour (*a*) $L = 2\frac{1}{2}\pi$, (*b*) $L = 6\pi$; initial disturbances are dotted. The pressure within each of the lobes is almost constant; the small lobes are slowly draining into their larger neighbours.

two lobes, perturbations with height comparable to the gap thickness $O(\bar{\epsilon})$ and length $O(\bar{\epsilon}^{\frac{1}{2}})$ relax in time $O(\bar{\epsilon}^{-1})$. Finally the timescale for changes due to volume exchange between the lobes must be estimated. Equation (3.44) can be written as $H_t = -Q_z$, so the rate of change of volume of a lobe lying between z_- and z_+ is

$$\frac{\mathrm{d}V}{\mathrm{d}t} = -2\pi(Q(z_+) - Q(z_-)). \tag{4.6}$$

Q is given by (3.43) and is $O(\bar{\epsilon}^{\frac{5}{2}})$ in the gap region. For a lobe of height $O(\bar{\epsilon}^{\frac{1}{2}})$ (4.6) then yields the drainage time as $O(\bar{\epsilon}^{-2})$.

Adjustments due to drainage take place much more slowly than the relaxation of disturbances in the lobes or gap. So, in modelling the drainage process, we may take the lobe and gap interface shapes to be steady. This means that the lobes will have the form (4.3), and, prompted by the observations of §4.2, we take the draining lobe as

$$H = \bar{\epsilon}^{\frac{1}{2}}(A + B\cos z) \quad (-z_0 < z < z_0), \tag{4.7}$$

where $H(-z_0) = H(z_0) = 0$ and $A, B = O(1)$, and the larger growing one as

$$H = C(1 - \cos(z - z_0)) \quad (0 < z - z_0 < 2\pi), \tag{4.8}$$

with $C = O(1)$. Integrating (4.10) from $\xi = -\Xi$ to Ξ with $|\Xi| \gg 1$ we obtain

$$\int_{-\Xi}^{\Xi} h_{\xi\xi\xi}\,\mathrm{d}\xi = [h_{\xi\xi}]_{-\Xi}^{\Xi} = q\int_{-\Xi}^{\Xi} h^{-3}\,\mathrm{d}\xi.$$

This last expression is non-zero when $q \neq 0$ because h is one-signed. Suppose now that both lobes tend linearly to zero at z_0. Matching of lobes and gap requires that h varies linearly with ξ for large $|\xi|$. However, then $[h_{\xi\xi}]_{-\Xi}^{\Xi} = 0$, a contradiction unless $q = 0$. It is not possible for a pair of lobes, one draining into the other, both to have finite slope as they approach the gap region. At least one lobe must have a quadratic zero at z_0, but the author has not been able to prove that both lobes cannot tend quadratically to zero. However, except in the special case of equal lobes such behaviour was not seen in the numerical solutions.

This observation has important consequences for the long-time behaviour of (3.44).

Any lobe of the form (4.3) tending quadratically to zero has axial length 2π, independent of the magnitude of its volume or pressure. Further, the greatest separation between neighbouring lobes of that form is 2π, at least while the region separating them is piecewise-described by (4.7) and (4.10). This follows because two lobes with quadratic zeros must be separated by one or more lobes which tend linearly to zero, the maximum length of each of which is 2π. But we have just shown that it is impossible for two lobes with linear zeros to be joined by a gap region which satisfies (4.10). Hence there is at most a single lobe with linear zeros joining each pair of lobes with quadratic zeros and so their spacing cannot be more than 2π. For very large times and large values of L there is some numerical evidence that the solution structure embodied in (4.7), (4.8) and (4.10) is no longer valid. However, the arguments given above remain true at moderately large times, and it seems reasonable to expect that the structures which develop then give some clue to the form of the long-time solutions.

Introducing scaled variables

$$\xi = \frac{z-z_0}{\bar{\epsilon}^{\frac{1}{3}}}, \quad h(\xi) = \frac{H(z,t)}{\bar{\epsilon}} \tag{4.9}$$

to describe the gap region, we find from (3.44) that steady shapes $h(\xi)$ satisfy

$$h_{\xi\xi\xi} = \frac{q}{h^3}. \tag{4.10}$$

q is a constant and $O(1)$ and the volume flux through the gap is

$$Q(z_0) = \tfrac{1}{3}\bar{\epsilon}^{\frac{1}{3}}q. \tag{4.11}$$

For simplicity we consider only periodic sets of lobes so that $Q(-z_0) = -Q(z_0)$.

Equation (4.10) must be supplemented with boundary conditions describing the matching of the gap and lobe region interfaces. From (4.8) we have

$$h \sim \frac{C}{2}\xi^2 \quad \text{as} \quad \xi \to \infty. \tag{4.12}$$

Turning now to (4.7), we have

$$H(z) \sim -\bar{\epsilon}^{\frac{1}{3}}\alpha(z-z_0) \quad \text{when} \quad -1 \ll z-z_0 \ll 0, \tag{4.13}$$

where

$$\alpha = -\frac{\mathrm{d}}{\mathrm{d}z}(A + B\cos(z))_{z=z_0} = O(1). \tag{4.14}$$

Rewriting (4.13) in terms of h and ξ, we obtain

$$h \sim -\alpha\xi \quad \text{as} \quad \xi \to -\infty, \tag{4.15}$$

justifying the earlier assertion that $H = O(\bar{\epsilon}^{\frac{1}{3}})$ in the draining lobe. (4.10), (4.12) and (4.15) can be put into universal form by writing

$$X = \frac{C}{2\alpha}\xi, \quad Y(X) = \frac{C}{2\alpha^2}h(\xi), \quad \Lambda = \frac{Cq}{2\alpha^5}, \tag{4.16}$$

in which case we have

$$Y_{XXX} = \frac{\Lambda}{Y^3}, \quad Y \sim X^2 \quad \text{as} \quad X \to \infty, \quad Y \sim -X \quad \text{as} \quad X \to -\infty. \tag{4.17}$$

This nonlinear eigenvalue problem can be solved numerically using a shooting method, giving $\Lambda = 0.60(5)$, as can also be deduced from the computations of Jones & Wilson (1979, Appendix B). Figure 5 shows the computed gap-shape function $Y(X)$.

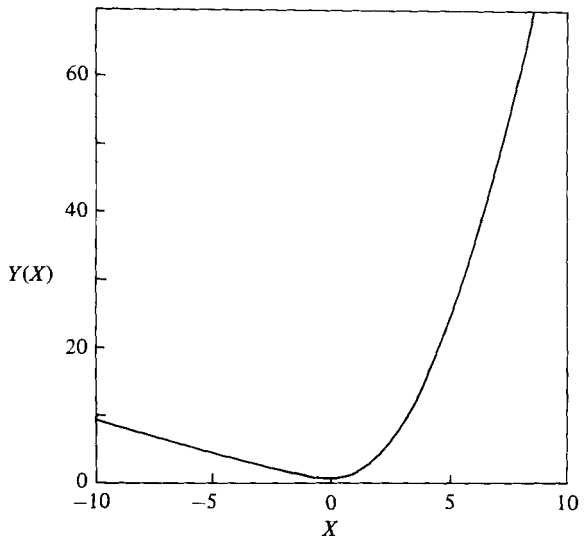

FIGURE 5. Universal gap shape function $Y(X)$.

We can now form an equation for the rate of change of volume of the draining lobe. A straightforward integration of (4.7) gives

$$V = 4\pi\bar{\epsilon}^{\frac{1}{2}}(1 - z_0 \cot z_0)\,\alpha, \tag{4.18}$$

and then rewriting (4.6) we obtain

$$\frac{\mathrm{d}V}{\mathrm{d}t} = -\frac{4A}{3C}(4\pi(1 - z_0 \cot z_0))^{-5} V^5 = -KV^5. \tag{4.19}$$

C and z_0 are $O(1)$ and change by at most $O(\bar{\epsilon}^{\frac{1}{2}})$ as the small lobe drains, so we take both equal to their values at $t = 0$. Equation (4.19) can then be integrated to give

$$V(t) = V(0)\,(1 + 4\,V(0)^4 Kt)^{-\frac{1}{4}}. \tag{4.20}$$

Complete drainage of the small lobe occurs, although it takes an infinitely long time.

The long-time solution structure described above was observed in the numerical results for values of $L \leqslant O(8\pi)$, although only in the 400-point computations was the spacial resolution sufficient that the $t^{-\frac{1}{4}}$ decay of the small-lobe volume could be seen. For larger values of L, although an initial disturbance breaks up after sufficient time into large lobes of length 2π separated by regions of length $\leqslant 2\pi$ as described above, after very long times these separating regions no longer seem to be of the form (4.7). Rather, they consist of a small lobe of that form together with a region where H is small and approximately uniform. The complete length of each of these regions is close to 2π, but in some cases somewhat greater. This behaviour is associated with translation of the large lobes in the z-direction, which is not possible in the strongly constrained small-L solutions. There seems to be a tendency for a large lobe to move towards its neighbour with the more negative internal pressure. However, for as long as the numerical integrations were pursued the small lobes drained into their larger neighbours and the large lobes remained separate, their spacing never becoming much greater than 2π.

More accurate numerical work or an extension of the analysis given above are needed to explain this very-long-time behaviour. However, in a real system, as the

film thins, the various additional physical effects discussed in §5.2 will come into play, invalidating this simple model long before the subtle long-time behaviour noted above occurs.

5. Discussion

5.1. *Summary*

When the effects of walls are negligible, fluid threads break up under surface tension into a number of spherical droplets. When there are confining walls close by, the interface is still unstable, although now in the nonlinear development the thread remains connected and it is the outer film which breaks up into a number of isolated lobes.

This instability and the final steady state can be successfully analysed using a thin-film approximation. While the thickness of the lobes formed cannot be predicted without full knowledge of the initial conditions, their axial extent is determined and is $2\pi a$. This lengthscale appears because the lobes must be axially symmetrical constant-pressure surfaces. It is geometrical rather than dynamical in origin, but has the kinematical consequence that fluid is transported only a finite distance along the film. Thermodynamic analyses of thread stability leading to the requirement of surface-area minimization can be misleading unless the correct constraints are applied. We must demand not only that total fluid volume is conserved but also that film fluid is not transported over distances much greater than $2\pi a$. A shape which gives a global area minimization may not be accessible in a continuous time evolution from a given initial state, and it is only by considering dynamical processes that accessibility can be determined. Capillary condensation (Everett & Haynes 1972) used as a model for the equilibrium distribution of phases in a porous medium may be criticized on the same grounds. The constraints on fluid rearrangement imposed by the mechanics of incompressible viscous flow with moving interfaces are different from, and more restrictive (even in non-axisymmetric geometries) than, those imposed by transport through successive evaporation and condensation.

In the process discussed here, fluid is gathered up into each lobe from within an axial length of about $4\pi a$ (each lobe has length $2\pi a$ and the greatest distance between lobes is also $2\pi a$). As a result, the film thickness can only be increased locally by a factor of about 4. For very thin outer films there is no possibility of this leading to snap-off of the core thread.

Over a wide range of viscosity ratios, the evolution of disturbances is controlled by the balance of surface-tension driving forces and viscous resistance in the outer fluid. The core fluid responds passively to the motion of the interface. Despite the ϵ^3 factor in (3.5), these adjustments do not take place so slowly as to be unobservable. If the tube radius is 100 μm, typical of rock pores and some laboratory experiments, then for $\epsilon = O(10^{-2})$ and γ, μ typical of water–oil systems (3.5) gives $T_{\text{film}} = O(10\text{ s})$, and, for larger values of ϵ, T_{film} decreases rapidly. For all except the slowest processes, time-dependent effects may be important.

5.2. *Neglected physical effects*

As the outer film thins, a number of neglected physical and physicochemical effects will become important. Forces due to electric double layers and van der Waals interactions will be significant when the film thickness is less than $O(0.1\ \mu\text{m})$. In the very late stages of adjustment, attractive forces will assist the film break-up (Williams

& Davis 1982), whereas a net repulsion will prevent the final complete disconnection of adjacent lobes (Chen & Slattery 1982). In either case the initial development of the instability, when the film is not too thin, will be unaffected.

Because surface tension alone can lead to the break-up of the film, we must be careful in interpreting observations of fluid configurations in terms of inhomogeneities in the wall wetting properties. Even on a chemically homogeneous pipe wall, a non-uniform film fluid distribution will develop.

Surfactants are undoubtedly present in real oil–water–rock systems, and non-uniformities in their concentration will lead to variations in surface tension along the interface. These will set up flows which may significantly change the behaviour found above. If we assume that the surfactant is soluble in the core fluid, and that the rate of diffusion from the bulk to the interface controls surfactant adsorption there, some measure of concentration non-uniformities is given by the Péclet number $\mathbb{P} = a|\boldsymbol{U}|/D$, where D is the diffusivity of a surfactant molecule in the bulk core fluid. If $\mathbb{P}$ is much greater than 1, we expect significant concentration gradients to develop along the interface because non-uniform advection of surfactant in the interface is stronger than the equilibrating effect of diffusion from the bulk. For the parameter values discussed above, $D = O(10^{-6}\ \mathrm{cm^2\ s^{-1}})$ typical of a small molecule, and $\epsilon = O(10^{-2})$, $\mathbb{P} = O(10)$ and in practice can be larger because the surfactant molecules may be limited to two-dimensional diffusion in the interface. Surface-tension non-uniformities are likely to be important, and the calculations described here must be reworked to discover their effects.

The flow channels ('pores and throats') in a real porous medium bear little resemblance to the uniform capillaries discussed here. They are neither straight, axisymmetric nor of uniform radius, and it is natural to ask whether the results of this detailed analysis are of any value in predicting interface behaviour in such geometries. Provided the pores and throats are such that there is a thin outer film separating the core from the pipe wall, the methods described here can be extended to study thread snap-off in constricted axisymmetric pipes (Hammond 1982, and a forthcoming paper), and to examine the effects of $O(\epsilon a)$ wall roughness and non-axisymmetry. And, even when a thin-film analysis is not strictly appropriate, qualitative ideas based on these studies may be useful.

The strong H^3 nonlinearity in the volume-flux expression (3.43) suggests that even small departures from axisymmetry will lead to significant changes in flow rate and the emergence of preferential flow paths where the film is thickest. When the surrounding pipe is strongly non-axisymmetric, so that there are $O(a)$ variations in the thickness of the outer fluid layer, we expect most of the fluid rearrangement to take place through these wide regions. Transport in any thin parts of the layer will be slow, because of the high resistance to flow, and the evolution of the interface initially at least will be controlled by the dynamics of the core and the widest parts of the outer layer. As in unbounded fluid, there is a strong possibility of snap-off, although the constraining effects of the walls may prevent the break-up of the thread into spheres. Flows in the thin parts of the outer layer may still control the long-time adjustment.

The analysis given above shows that axisymmetric capillaries are poor models from which to deduce the equilibrium phase distributions within single pores in a porous medium. In axisymmetric capillaries, after an initial adjustment, the film breaks up into disconnected lobes and no further outer-fluid transport is possible. This localization property is special to axisymmetric geometries. There is no reason to expect similar behaviour in the more realistic non-axisymmetric case. Even after

adjustment, connected surface films will then remain, along which the outer fluid can be transported over large distances.

5.3. *Break-up of threads surrounded by moderately thin films*

Goldsmith & Mason (1963) report the break-up of very long bubbles in circular capillary tubes. We have already shown that such behaviour cannot occur if the outer fluid film is very thin, and it is of interest to attempt to predict at what thickness snap-off is possible. This cannot be done within a thin-film approximation of course, but we can give a qualitative argument using some of the ideas developed above.

If the inner thread is to snap, sufficient fluid must be collected together to form a lenticular bridge across the pipe. The interfaces of such a bridge are opposing hemispherical caps of radius a and the least volume that can be enclosed between them is $\frac{2}{3}\pi a^3$. For thin films the total amount of fluid gathered up is approximately (circumference of pipe) $\times$ (thickness of film) $\times$ (length of film from which fluid is collected) $= O(8\pi^2\epsilon a^3)$. Snap-off is impossible if this is less than $\frac{2}{3}\pi a^3$, so when $\epsilon < 1/12\pi \approx 0.03$ the core thread must remain connected. If ϵ is bigger than this value, but still sufficiently small for thin-film theory to be valid, we expect the initial stages of adjustment to be much as described above. But, as Everett & Haynes (1972) have shown, when the lobe volume becomes greater than a certain value, its surface area is bigger than that of a lens bridging the pipe. On thermodynamic grounds we then expect the interface to tend towards that shape, although the geometrical approximations made prevent the thin-film theory given here from showing such behaviour.

Any droplet formed in thread break-up must have surface area less than part of the original thread with the same volume. Together with the restriction for moderately thin films that outer fluid cannot be transported more than a distance of about $2\pi a$, this gives another bound on ϵ for the occurrence of snap-off. Taking the very crudest model of a droplet after snap-off as a cylindrical middle section of length L and radius a with hemispherical endcaps also of radius a (as in the previous paragraph), elementary calculations show that surface area reduction requires $L/a > 2/3\epsilon - 2$. But the total droplet length is bounded above by the distance between neighbouring lobes which is constrained by the film-fluid readjustment processes to be less than $4\pi a$. This fixes $L + 2a < 4\pi a$, and hence $\epsilon > 1/6\pi$ if snap-off is to occur. While it would be unwise to put too much faith in the numerical values of these estimates, they are based on a realistic model of the underlying dynamics which indicates how volume conservation constraints and the interaction between flow and variable geometry prevents threads surrounded by thin films from breaking up.

Most of the work described here was done while the author was a research student in DAMTP, Cambridge University. He is grateful to Dr E. J. Hinch for many suggestions and shared insights, to the SERC for financial support and to Professor J. R. A. Pearson for his criticism of an earlier version of this paper.

Appendix

When $\lambda = O(h/a)^{-1}$ the asymptotic structure described in §3.2 breaks down because then the perturbation flow in the film driven by the core tangential stress at the interface is as large as the basic film flow. Order-of-magnitude arguments following the pattern of §3.1 suggest that the flow field takes the following forms as λ increases.

When $(h/a)^{-1} \ll \lambda \ll (h/a)^{-2}$ the film axial and radial velocity components and pressure gradient are estimated as before by (3.6) and (3.7). However, now $w = 0$ at the interface (at leading order) and the major response in the core to this film flow is driven by the tangential stress exerted by the film at the interface. The core velocity then has $|\boldsymbol{U}| = O(\lambda^{-1}(h/a)^2\gamma/\mu)$ with associated stresses $|\boldsymbol{\Sigma}| = O((h/a)^2\gamma/a)$. The radial component U of core velocity vanishes at the interface, but Σ_{nn} and W are non-zero there. They set up small corrections in the film with axial velocities $O((h/a)w)$ and $O(\lambda^{-1}(h/a)^{-1}w)$ respectively. The non-zero film radial velocity component drives a correction of size $O(\lambda(h/a)^2|\boldsymbol{U}|)$ in the core which is as large as the basic core flow when $\lambda = O(h/a)^{-2}$, signalling the breakdown of this asymptotic structure.

When $(h/a)^{-2} \ll \lambda \ll (h/a)^{-3}$ the following picture emerges. Film velocities and pressures are still estimated by (3.6) and (3.7) and $w = 0$ at the interface. The major response in the core is now driven by the film radial velocity component u, leading to a core flow with $|\boldsymbol{U}| = O((h/a)^4\gamma/\mu)$ and $|\boldsymbol{\Sigma}| = O(\lambda(h/a)^4\gamma/a)$. The core tangential stress Σ_{nt} vanishes at the interface. The core axial velocity drives an $O((h/a)w)$ perturbation flow in the film, and the film tangential stress sets up a small correction in the core with velocities $O(\lambda^{-1}(h/a)^{-2}|\boldsymbol{U}|)$. Core normal stresses set up a pressure perturbation in the film which drives an $O(\lambda(h/a)^3 w)$ correction flow there. Notice that when $\lambda(h/a)^3 = O(1)$ this is as large as the basic film flow, and core pressures are as large as the film-pressure fluctuations, which, up to this value of λ, have dominated the normal-stress balance and driven the flow.

Finally, when $\lambda \gg (h/a)^{-3}$ the dynamics of the core region control the flow. Core-pressure variations are $O((h/a)\gamma/a)$ with associated velocities $|\boldsymbol{U}| = O(\lambda^{-1}(h/a)\gamma/\mu)$ and stresses $|\boldsymbol{\Sigma}| = O((h/a)\gamma/a)$. The core tangential stress Σ_{nt} vanishes at the interface. The core radial velocity component U is non-zero there and drives the major response in the film, setting up a flow with $u = O(\lambda^{-1}(h/a)\gamma/\mu)$, $w = O(\lambda^{-1}\gamma/\mu)$ with $w = 0$ at the interface and $p_z = O(\lambda^{-1}(h/a)^{-2}\gamma/a^2)$. The tangential and normal components of stress in the film drive perturbations in the core with velocities $O(\lambda^{-1}(h/a)^{-2}|\boldsymbol{U}|)$ and $O(\lambda^{-2}(h/a)^{-2}|\boldsymbol{U}|)$ respectively. As $\lambda \to \infty$ all these perturbations remain small compared with the main flows. Recalling the results of §3.1, we see that when $h/a \ll 1$ a complete set of four distinct asymptotic structures has been found as λ varies.

Repeating the formal analysis of §3.2 for

$$(h/a)^{-1} \ll \lambda \ll (h/a)^{-2} \quad \text{or} \quad (h/a)^{-2} \ll \lambda \ll (h/a)^{-3},$$

we find that lubrication theory may be used to describe the film flow which can again be found without calculating the complete core flow. In both cases the film axial velocity $w_0 = \frac{1}{2}p_{0z}(y^2 - Hy)$, with p_0 given by (3.40). The interface evolution equation is then the same as (3.44), but with the numerical factor of $\frac{1}{3}$ replaced by $\frac{1}{12}$. The main difference between these two viscosity-ratio regimes is in the way in which film and core interact. As a consequence the core flows differ, but the film flows, and hence the behaviour of the interface, are the same in both cases. The dynamics of the film region control the flow and are, within the lubrication approximation, independent of the details of the core flow. This is reflected in the results of the linearized stability analysis, where no distinction appears between $(h/a)^{-1} \ll \lambda \ll (h/a)^{-2}$ and $(h/a)^{-2} \ll \lambda \ll (h/a)^{-3}$, (2.24) covering both regimes. In figure 2 we see a single extended region where the growth rate is independent of λ for each value of h/a and $1 \ll \lambda(h/a) \ll (h/a)^{-2}$.

For very large core viscosities, $\lambda \gg (h/a)^{-3}$, the timescale for interface adjustments is given by $T_{\text{core}} = O(\lambda a\mu/\gamma)$, using the above velocity estimates. This behaviour can

be seen in figure 2, where for the largest values of λ all the maximum growth rate curves fall away with slope -1. The core flow alone determines the motion of the interface and the methods of linearized analysis can be used to trace its evolution until it has come sufficiently close to the wall for film pressures to be significant.

REFERENCES

CHEN, J. D. & SLATTERY, J. C. 1982 *AIChE J.* **28**, 955.

EVERETT, D. H. & HAYNES, J. M. 1972 *J. Coll. Interface Sci.* **38**, 125.

GOLDSMITH, H. L. & MASON, S. G. 1963 *J. Coll. Interface Sci.* **18**, 237.

GOREN, S. L. 1962 *J. Fluid Mech.* **12**, 309.

HALL, G. & WATT, J. M. (eds.) 1976 *Modern Numerical Methods for Ordinary Differential Equations*. Oxford University Press.

HAMMOND, P. S. 1982 Flows driven by surface tension with nearby rigid boundaries. PhD dissertation, Cambridge University.

HAPPEL, J. & BRENNER, H. 1965 *Low Reynolds Number Hydrodynamics*. Prentice-Hall.

HICKOX, C. E. 1971 *Phys. Fluids* **14**, 251.

JONES, A. F. & WILSON, S. D. R. 1978 *J. Fluid Mech.* **87**, 263.

KOPLIK, J., WILKINSON, D. & WILLEMSEN, J. F. 1983 Percolation and capillary fluid displacement. *Presented at the Workshop on the Mathematics and Physics of Disordered Media, University of Minnesota, February 1983.*

LARSON, R. G., SCRIVEN, L. E. & DAVIS, H. T. 1981 *Chem. Engng Sci.* **36**, 57.

MOHANTY, K. K. 1981 Fluids in porous media: two phase distribution and flow. PhD dissertation, University of Minnesota.

RAYLEIGH, LORD 1892 *Phil. Mag.* **34**, 145.

TAYLOR, G. I. 1934 *Proc. R. Soc. Lond.* A **146**, 501.

TAYLOR, G. I. 1961 *J. Fluid Mech.* **10**, 161.

TOMOTIKA, S. 1935 *Proc. R. Soc. Lond.* A **150**, 322.

WILLIAMS, M. B. & DAVIS, S. H. 1982 *J. Coll. Interface Sci.* **90**, 220.

WU, R. & WEINBAUM, S. 1982 *J. Fluid Mech.* **121**, 315.